DESY 12-137
HU-EP-12/24
JLAB-THY-12-1606
SFB/CPP-12-55

A quenched study of the Schrödinger functional with chirally rotated boundary conditions: applications

J. González López [a,b], K. Jansen [b], D. B. Renner [c], A. Shindler [a 1]

[a] *Humboldt-Universität zu Berlin, Institut für Physik Newtonstrasse 15, 12489 Berlin, Germany*

[b] *DESY,Platanenallee 6, 15738 Zeuthen, Germany*

[c] *Jefferson Lab, 12000 Jefferson Avenue, Newport News, VA 23606, USA*

Abstract

In a previous paper [1], we have discussed the non-perturbative tuning of the chirally rotated Schrödinger functional (χSF). This tuning is required to eliminate bulk O(a) cutoff effects in physical correlation functions. Using our tuning results obtained in [1] we perform scaling and universality tests analyzing the residual O(a) cutoff effects of several step-scaling functions and we compute renormalization factors at the matching scale. As an example of possible application of the χSF we compute the renormalized strange quark mass using large volume data obtained from Wilson twisted mass fermions at maximal twist.

[1] Heisenberg Fellow

24 August 2012

1 Introduction

The Schrödinger functional (SF) scheme [2,3,4] has been widely employed for performing non-perturbative renormalization and scaling studies. For an incomplete list of references see [5,6,7,8,9,10,11,12,13].

It is not straightforward to implement a Schrödinger functional (SF) scheme that retains the property of automatic O(a) improvement [14] for massless Wilson fermions. A solution to this problem has been proposed recently by Sint [15], called chirally rotated Schrödinger functional (χSF). In refs. [16,17,18] preliminary studies of the χSF were presented and recently in a companion paper [1] we have performed a detailed study of the non-perturbative tuning of the χSF in a quenched setup. To retain the property of bulk automatic O(a) improvement two parameters of the lattice action, one denoted by z_f and the other, hopping paramter κ, have to be tuned non-perturbatively to their critical values.

In ref. [1] we have defined a tuning procedure and we have found that the tuning of z_f and κ is numerically feasible with standard techniques. We have found that several different tuning conditions lead to fully compatible results for all physical correlation functions and we have also numerically checked that in the continuum limit the correct boundary conditions, i.e. the boundary conditions needed to have bulk automatic O(a) improvement, are recovered.

The χSF being compatible with automatic O(a) improvement can hence be used for renormalizing bare operators computed with Wilson twisted mass fermions at maximal twist [19]. In this paper we discuss the application of the χSF renormalization scheme for the determination of several physically relevant quantities. The computation of such quantities will moreover allow us to perform a test of the universality of the continuum limit of lattice QCD and, as a result, to confirm the correctness of the continuum limit of the novel χSF scheme itself. The latter can be achieved by comparing the continuum limit values of the computed quantities in the χSF formulation to those values obtained using the standard version of the SF. Since, as discussed in ref. [1], the SF and the χSF are the same formulations in the continuum, the final results in the continuum limit, as obtained from the two formulations, should be exactly the same given a common choice of a renormalization prescription.

The paper is organized as follows. We discuss the continuum limit of the step scaling function (SSF) of the pseudo-scalar density, $\sigma_{\rm P}$ in sect. 2 and of the non-singlet twist 2 operators, $\sigma_{\rm O_{12}}$ and $\sigma_{\rm O_{44}}$, in sect. 3. The continuum limit values are then compared to the ones obtained using the SF, with which, as expected, we find an agreement. Next, in sec. 4 we show the results in the determination of the renormalization factors of the pseudo-scalar density, $Z_{\rm P}$, and the twist 2 operators, $Z_{\rm O_{12}}$ and $Z_{\rm O_{44}}$, at the matching scale with hadronic schemes and non-zero lattice spacing. For the latter, results are compared against values

obtained using the standard formulation of the SF with two different regularizations, non-improved Wilson and clover improved Wilson fermions. Eventually in sec. 5 we compute the running strange quark mass, using the values of $Z_{\rm P}$ obtained from the χSF scheme and the tuned bare quark mass obtained using twisted mass Wilson fermions at maximal twist. We compare our findings with the strange quark mass obtained using standard SF as a renormalization scheme and non-perturbatively improved Wilson fermions. All these results are, therefore, a demonstration of the correctness of the continuum limit of the χSF renormalization scheme and, consequently, of its applicability in the determination of renormalization factors.

The analysis presented in this paper relies substantially on the results obtained in ref. [1]. We therefore assume from now on that the reader is familiar with that paper and the notation adopted that will be taken over without further notice. Additionally all the equations of ref. [1] will be denoted by the equation number prefixed by I as for example (I.5.10).

2 Step scaling functions: pseudoscalar density

The step scaling function (SSF), $\sigma_{\rm O}$, of a certain scale-dependent observable, $O(L)$, describes the behavior of $O(L)$ under changes in the value of the renormalization scale, $\mu = 1/L$, where L denotes the linear extent of the finite volume. The reason SSFs are good candidates to perform universality tests is that they are finite quantities which depend upon the renormalization scheme and the renormalization prescription employed. While at finite value of the cutoff, SSFs are regularization-dependent, after the removal of the cutoff they are independent from the regulator.

Let us discuss the concept of the SSF, with the example of the the normalization $Z_{\rm P}$ of the pseudoscalar density. The evolution of $Z_{\rm P}$ from a scale L to sL is described by the step scaling function according to

$$Z_{\rm P}(L)\sigma_{\rm P}(s,\overline{g}^2(L)) = Z_{\rm P}(sL)\,, \tag{2.1}$$

where the $\overline{g}^2(L)$ represents the renormalized coupling at the scale L. Since in this way the running of the coupling itself enters the SSF, for the computation of any SSF, the previous knowledge of the SSF of the gauge coupling is hence needed. In this work, where the quenched setup is chosen and the gauge action is the Wilson gauge action there is no need in recomputing the renormalized gauge coupling and its corresponding SSF. These are already known from previous publications [5,6,20] for a very wide range of energies. If a different gauge action and/or dynamical fermions are included, the gauge coupling would need to be recomputed within the new setup.

The previous discussion refers to the formal continuum theory. Going to a hypercubical

lattice with spacing a, the chosen renormalization condition for the pseudoscalar density in the χSF scheme is the following,

$$Z_{\rm P}(g_0, L/a) = c(\theta, a/L)\, \frac{\sqrt{g_1(\theta)}}{g_{\rm P}(L/2,\theta)}\Big|_{m=0}\,. \tag{2.2}$$

In this expression, $m = 0$ indicates that the renormalization condition is imposed at zero quark mass. In our case, corresponding to Wilson fermions, this means at the critical value of the bare quark mass, $m_0 = m_{\rm cr}$, as determined from the tuning in ref. [1]. The factor $c(\theta, a/L)$ is chosen such that $Z_{\rm P}$ takes the correct value at tree-level, $Z_{\rm P}(0, L/a) = 1$. Therefore it is defined as

$$c(\theta, a/L) \equiv \frac{g_{\rm P}(L/2,\theta)}{\sqrt{g_1(\theta)}}\Big|^{\rm tree}_{m_0=0}\,. \tag{2.3}$$

The two-point functions entering the definition of $Z_{\rm P}$ have already been discussed in ref. [1]. They are recalled here for better readability

$$g_{\rm P}(x_0,\theta) \equiv g^{11}_{\rm P\_}(x_0,\theta) = -\frac{a^3}{L^3}\sum_{\mathbf{x}}\langle P^1(x)\widetilde{\mathcal{P}}^1_-\rangle\,, \tag{2.4}$$

with P^1 denoting the pseudoscalar density, and

$$g_1(\theta) \equiv g_1^{11}(\theta) = -\frac{1}{L^6}\,\langle \widetilde{\mathcal{P}'}^1_+ \widetilde{\mathcal{P}}^1_-\rangle\,. \tag{2.5}$$

See ref. [1] for the exact definitions of the quantities in eqs. (2.4,2.5). In order to determine the renormalization prescription completely, a value of θ has to be chosen. In particular, we consider here two cases, $\boldsymbol{\theta} = (0.5, 0.5, 0.5)$ and $\boldsymbol{\theta} = (1, 0, 0)$.

Given a fixed value of the renormalization scale, defined through $\overline{g}^2(L) = u$, and a fixed value of the lattice spacing, leading hence to a fixed value of L/a, the lattice SSF of the pseudoscalar density is given by

$$\Sigma_{\rm P}(s, u, a/L) = \frac{Z_{\rm P}(g_0, sL/a)}{Z_{\rm P}(g_0, L/a)}\Big|_{m=0,\,\overline{g}^2(L)=u}\,. \tag{2.6}$$

In the continuum limit, the SSF is finite and takes the value

$$\sigma_{\rm P}(s, u) = \lim_{a\to 0}\Sigma_{\rm P}(s, u, a/L)\,. \tag{2.7}$$

From the definition of the SSF, eq. (2.6), it is understood that in order to compute the SSF at a certain value of the renormalization scale, $1/L$, the Z-factor needs to be evaluated both at L and sL, for a fixed value of the lattice spacing. In particular here we always use $s = 2$. This means that, for a fixed value of a (equivalently $\beta = \frac{6}{g_0^2}$), simulations have to be performed at a certain value of $L/a = N$ (small lattices) and also at $2L/a = 2N$

(double lattices). In such computations, the values of all parameters, e.g. $\kappa_{\rm cr}$ and z_f^c, are the same at L and $2L$ for a fixed value of the lattice spacing, since such parameters only depend on the bare coupling. This is important because it implies that the tuning of the parameters only needs to be performed at the 'single' and hence smaller lattices.

We summarize the results for $Z_{\rm P}$ in tab. A.1, at $\boldsymbol{\theta} = (0.5, 0.5, 0.5)$ and $\boldsymbol{\theta} = (1, 0, 0)$. Results at three different values of the renormalization scale are presented; the hadronic scale $L = 1.436\, r_0$, the intermediate scale $\overline{g}^2 = 2.4484$ and the perturbative scale $\overline{g}^2 = 0.9944$. The computation of the SSF will be performed at only the intermediate and the perturbative scales. We use the results for $Z_{\rm P}$ at the hadronic (matching) scale for the calculation of the renormalized strange quark mass as it will be discussed in sec. 5. All results presented in the present and following chapters have been obtained using the critical values of the parameters, $\kappa_{\rm cr}$ and z_f^c, as determined from the tuning condition (1*) (cf. ref. [1]).

From the data in tab. A.1 we have computed the SSF on the lattice, for each lattice spacing at the intermediate and perturbative scales. The results are presented in tab. A.2 for $\boldsymbol{\theta} = (0.5, 0.5, 0.5)$ and tab. A.3 for $\boldsymbol{\theta} = (1, 0, 0)$. In tab. A.2 we also show the results obtained from the SF with improved and standard Wilson fermions as taken from ref. [20]. These data are presented in columns 3 and 4 and denoted 'Clover' and 'Wilson', respectively.

For both the χSF and the SF with clover improved Wilson fermions we have performed the continuum limit with a linear fit of the SSF in $(a/L)^2$,i.e. using a form

$$y = c_0 + c_1 \left(\frac{a}{L}\right)^2 \tag{2.8}$$

while a linear fit in a/L for the SF with standard Wilson fermions was used

$$\bar{y} = \bar{c}_0 + \bar{c}_1 \left(\frac{a}{L}\right). \tag{2.9}$$

The results of our fits are summarized in tab. A.4 for $\boldsymbol{\theta} = (0.5, 0.5, 0.5)$ and in tab. A.5 for $\boldsymbol{\theta} = (1, 0, 0)$. In both tables we show the results at the two values of the renormalization scale that have been considered, $\overline{g}^2 = 2.4484$ and $\overline{g}^2 = 0.9944$. For comparison, in tab. A.4 we also present the continuum limit results for the SF with improved and standard Wilson fermions. We have performed our own fits of the data obtained from the SF, since in [20] there are no tables with the final continuum limit values, where we could read the data from.

A comparison of the SSF for the different kind of lattice fermions can be seen in fig. 1. Here we plot the data we have used for $\Sigma_{\rm P}$ (cf. tab. A.2) as a function of a/L for the three formulations. The corresponding values in the continuum limit are also shown (cf. tab. A.4). From this figure it becomes clear that the slopes, i.e. the values of c_1 and $\bar{c}_1$ in eqs. (2.8,2.9), are consistent with zero in the three cases. In particular, the data from the three regularizations agree in the continuum limit for both values of the renormalization

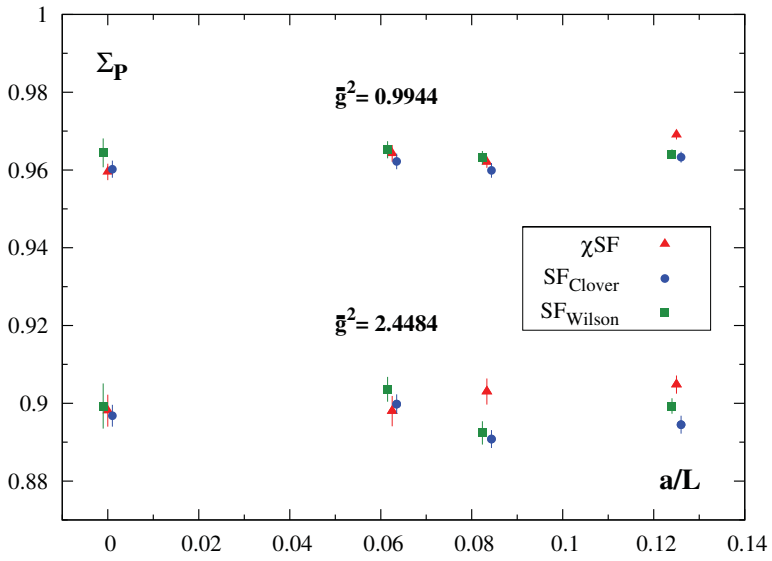

Fig. 1. Lattice SSF of the pseudo-scalar density and continuum limit values. Results are shown for the χSF with standard Wilson fermions and the SF with improved and standard Wilson fermions, at the intermediate and perturbative scales and for $\boldsymbol{\theta} = (0.5, 0.5, 0.5)$. The extrapolations to the continuum limit are performed according to tab. A.4: linear in $(a/L)^2$ for the χSF and the SF with improved fermions and linear in a/L for the SF with standard Wilson fermions. The data from the SF have been slightly displaced to the right and left, respectively, for the improved and the standard Wilson fermions formulations.

scale. Moreover, at non-zero lattice spacing the data for the three formulations agree at $L/a = 16$ for the intermediate scale and at $L/a = 12, 16$ for the perturbative scale.

In fig. 2 we show the extrapolation to the continuum limit of $\Sigma_{\rm P}$ as determined from the χSF, for the two values of $\boldsymbol{\theta}$ and the two values of $1/L$ that we have considered. The data are plotted as a function of $(a/L)^2$ and the corresponding values in the continuum limit, $\sigma_{\rm P}$, are also shown. The fitting curves are also plotted as dashed lines. Note that, for the two values of $\boldsymbol{\theta}$ employed in the definition of the renormalization prescription, the continuum limit values are not supposed to be compared. Different values of $\boldsymbol{\theta}$ give rise to different renormalization prescriptions and, as a consequence, the results are not expected to agree even in the continuum limit.

A similar plot is shown in fig. 3, where we present the results of the extrapolation to the continuum limit for the χSF and the improved SF, for comparison. Results are shown at the two values of the renormalization scale and for $\boldsymbol{\theta} = (0.5, 0.5, 0.5)$. Since the same renormalization prescription is chosen in both formulations, the continuum limit values should agree, between the SF and the χSF. As shown in the plot, this is indeed the case. Note that the slopes for the two formulations have similar absolute values but opposite

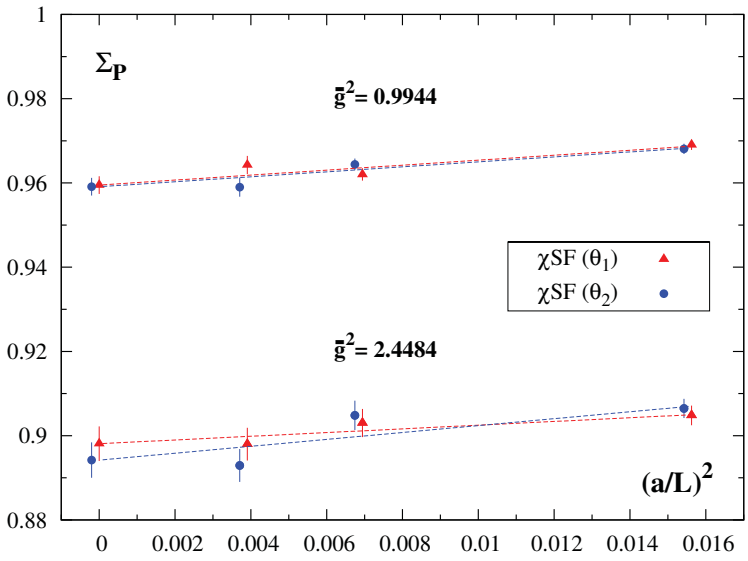

Fig. 2. Continuum limit extrapolation of the SSF of the pseudo-scalar density. Only χSF data are shown, both for $\theta_1 \equiv \boldsymbol{\theta} = (0.5, 0.5, 0.5)$ and $\theta_2 \equiv \boldsymbol{\theta} = (1, 0, 0)$, at the intermediate and perturbative scales. The extrapolations to the continuum limit are linear in $(a/L)^2$ as shown by dashed lines wich represents fits linear in $\left(\frac{a^2}{L^2}\right)$ to the data. See also tab. A.4 and tab. A.5. The values in the continuum limit are also plotted. The data from θ_2 have been slightly displaced to the left.

signs. This would allow in principle to perform a constraint fit to the continuum limit reducing the errors in the final results.

From all results presented here, we can conclude that the continuum limit of the SSF of the pseudoscalar density determined from the χSF agrees with the corresponding value obtained using the standard formulation of the SF, with and without improvement. Furthermore, we observe that the results already agree at finite lattice spacing, at $L/a = 16$ for $\overline{g}^2 = 2.4484$ and at $L/a = 12, 16$ for $\overline{g}^2 = 0.9944$. These results are therefore a successful test of the universality of the continuum limit. Moreover, the approach to the continuum limit is consistent with the expected leading $O(a^2)$ discretization effects in the χSF formulation, indicating that the χSF is indeed compatible with bulk automatic $O(a)$-improvement.

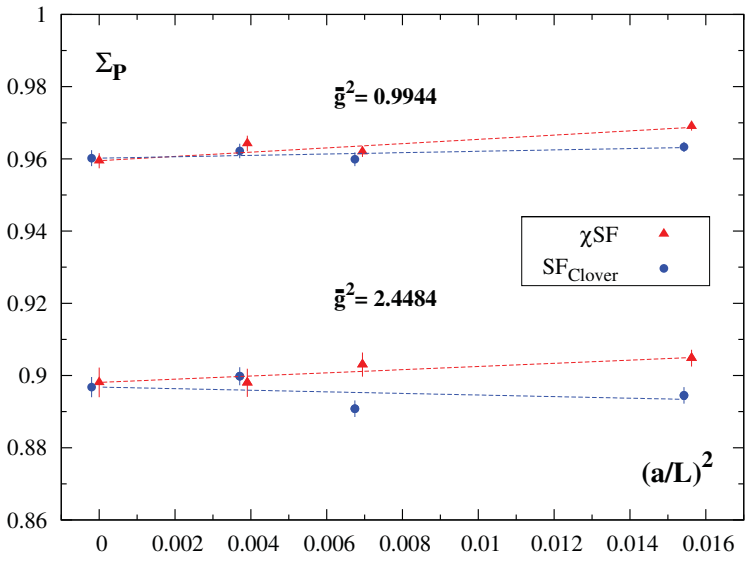

Fig. 3. Continuum limit extrapolation of the SSF of the pseudo-scalar density. Results are shown for the χSF with standard Wilson fermions and the SF with improved Wilson fermions, at the intermediate and perturbative scales and for $\boldsymbol{\theta} = (0.5, 0.5, 0.5)$. The extrapolations to the continuum limit represented as the dashed lines are linear in $(a/L)^2$ for all cases. The results from the fits are presented in tab. A.4. The data from the SF have been slightly displaced to the left.

3 Step scaling functions: twist-2 operators

The above discussion for the case of the pseudoscalar density can be directly translated to any other scale-dependent observable. In particular, we also compute here the SSF of non-singlet twist-2 composite fields made up of quark and anti-quark fields, related to the first moment (lowest moment) of unpolarized structure functions.

In Minkowski space the relevant twist-2 gauge-invariant composite operator reads

$$\mathrm{i}^{n-1}\,\overline{\psi}(x)\gamma_{\{\mu_1}\overleftrightarrow{D}_{\mu_2}\cdots\overleftrightarrow{D}_{\mu_n\}}\frac{\tau^a}{2}\psi(x) + \text{`trace terms'}\,. \tag{3.1}$$

The symmetrization in the Lorentz indices, $\{\ldots\}$, is required because we deal here with unpolarized scattering and the 'trace terms' (terms with $g_{\mu_i\mu_j}$) in order to provide the composite field with a definite spin. The covariant derivative, $\overleftrightarrow{D}_{\mu_i}$, is defined as the combination

$$\overleftrightarrow{D}_{\mu_i} = \frac{\overrightarrow{D}_{\mu_i} - \overleftarrow{D}_{\mu_i}}{2}\,, \tag{3.2}$$

with $\overrightarrow{D}_{\mu_i}$ and $\overleftarrow{D}_{\mu_i}$ the covariant derivatives acting to the right and left, respectively.

Since we compute quantities within the χSF scheme and we work in the twisted basis, we give here the expressions of the twist-2 operators in Euclidean space in the twisted basis explicitly. These can be obtained from the corresponding expressions in the physical basis, applying the standard axial rotation eq. (I.2.2) in the continuum theory and then directly translating the fields and derivatives to the lattice. Performing the rotation we obtain

$$O^a_{\mu\nu}(x) = \overline{\chi}(x)\, e^{\mathrm{i}\frac{\alpha}{2}\gamma_5\tau^3}\, \gamma_{\{\mu}\, \overleftrightarrow{D}_{\nu\}}\, \frac{\tau^a}{2}\, e^{\mathrm{i}\frac{\alpha}{2}\gamma_5\tau^3}\, \chi(x) \tag{3.3}$$

and depending on the flavor structure,

$$O^a_{\mu\nu}(x) = \begin{cases} \overline{\chi}(x)\, \gamma_{\{\mu}\, \overleftrightarrow{D}_{\nu\}}\, \left[\cos(\alpha)\, \frac{\tau^a}{2} + \epsilon_{ab3}\sin(\alpha)\, \gamma_5\, \frac{\tau^b}{2}\right]\chi(x) & (a=1,2)\,, \\ \\ \overline{\chi}(x)\, \gamma_{\{\mu}\, \overleftrightarrow{D}_{\nu\}}\, \frac{\tau^a}{2}\, \chi(x) & (a=3)\,, \end{cases} \tag{3.4}$$

with ϵ_{abc} the totally anti-symmetric tensor ($\epsilon_{123}=1$). In the particular case of maximal twist, $\alpha = \pi/2$, this expression reduces to

$$O^a_{\mu\nu}(x) = \begin{cases} \epsilon_{ab3}\, \overline{\chi}(x)\, \gamma_{\{\mu}\, \overleftrightarrow{D}_{\nu\}}\, \gamma_5\, \frac{\tau^b}{2}\, \chi(x) & (a=1,2)\,, \\ \\ \overline{\chi}(x)\, \gamma_{\{\mu}\, \overleftrightarrow{D}_{\nu\}}\, \frac{\tau^a}{2}\, \chi(x) & (a=3)\,. \end{cases} \tag{3.5}$$

These composite fields are scale-dependent quantities which need to be renormalized, $O_{\mathrm{R}} = Z_{\mathrm{O}}^{-1}\, O_{\mathrm{B}}$, with O_{B} the bare operator and Z_{O} its renormalization constant.

The corresponding SSF in the continuum $\sigma_{\mathrm{Z_O}}(s, \overline{g}^2(L))$ is defined as

$$Z_{\mathrm{O}}(sL) = \sigma_{\mathrm{Z_O}}(s, \overline{g}^2(L))\, Z_{\mathrm{O}}(L)\,. \tag{3.6}$$

Using a lattice as a regulator, lattice artifacts must be taken into account and therefore the renormalized operator is given as [2]

$$O_{\mathrm{R}}(L) = \lim_{a\to 0} Z_{\mathrm{O}}^{-1}(g_0, L/a)\, O_{\mathrm{B}}(g_0)\,. \tag{3.7}$$

Eventually we will compute boundary to bulk correlation functions, with the twist-2 operators inserted in the bulk of the lattice at a certain space-time point x. The boundary interpolating fields at $x_0 = 0$ that we consider here are, following [21], expressed in the physical basis,

$$a^6 \sum_{\mathbf{y},\mathbf{z}} \overline{\zeta}(\mathbf{y})\gamma_k \frac{\tau^a}{2}\zeta(\mathbf{z})\,. \tag{3.8}$$

[2] The definition of the renormalized operator with Z^{-1} is done to be consistent with the definitions used in ref [7].

Performing a rotation to the twisted basis, with maximal twist angle, such boundary interpolating fields take the form

$$\mathcal{O}^a_{\gamma_k} = \begin{cases} \epsilon_{ab3}\, a^6 \sum_{\mathbf{y},\mathbf{z}} \overline{\zeta}(\mathbf{y})\, \gamma_k \gamma_5 \frac{\tau^b}{2}\, \widetilde{Q}_-\, \zeta(\mathbf{z}) & (a = 1,2)\,, \\ \\ a^6 \sum_{\mathbf{y},\mathbf{z}} \overline{\zeta}(\mathbf{y})\, \gamma_k \frac{\tau^a}{2}\, \widetilde{Q}_-\, \zeta(\mathbf{z}) & (a = 3)\,. \end{cases} \tag{3.9}$$

In particular, we consider two cases for the gamma matrices at the boundaries, γ_k with $k = 1, 2$. The case $k = 1$ ($k = 2$) will be used when computing the correlation function of the operator O^a_{44} (O^a_{12}). Therefore, the correlation functions that we consider here are the following,

$$g_{12}(x_0, \theta) \equiv -\frac{a^9}{L^3} \sum_{\mathbf{x},\mathbf{y},\mathbf{z}} \langle \overline{\chi}(x)\, \gamma_{\{1}\, \overset{\leftrightarrow}{D}_{2\}}\, \gamma_5\, \frac{\tau^1}{2}\, \chi(x)\, \overline{\zeta}(\mathbf{y})\, \gamma_2 \gamma_5 \frac{\tau^1}{2}\, \widetilde{Q}_-\, \zeta(\mathbf{z}) \rangle\,, \tag{3.10a}$$

$$g_{44}(x_0, \theta) \equiv -\frac{a^9}{L^3} \sum_{\mathbf{x},\mathbf{y},\mathbf{z}} \langle \overline{\chi}(x)\, \gamma_{\{0}\, \overset{\leftrightarrow}{D}_{0\}}\, \gamma_5\, \frac{\tau^1}{2}\, \chi(x)\, \overline{\zeta}(\mathbf{y})\, \gamma_1 \gamma_5 \frac{\tau^1}{2}\, \widetilde{Q}_-\, \zeta(\mathbf{z}) \rangle\,. \tag{3.10b}$$

Note that we have chosen only the cases where the two flavor matrices, in the bulk and at the boundary, are the same and we have picked up only the component τ^1. The reason for choosing both matrices to be the same is that this is the only possibility for the correlation functions not to vanish, due to symmetry arguments. Amongst the three possibilites, $\tau^{1,2,3}$, all of them should provide the same value in the continuum limit. Due to our particular setup where flavor symmetry is broken at finite lattice spacing, there is a distinction between $\tau^{1,2}$ and τ^3. Even if in the case with τ^3 the expressions look simpler, because this correlation function does not rotate, the appearance of disconnected pieces, which are very costly from the numerical point of view, leads us to decide for the other cases $\tau^{1,2}$. Since these two cases are exactly equivalent, we select just τ^1.

We can now choose a renormalization prescription for the twist-2 operator within the χSF scheme. In particular we impose the renormalization condition

$$Z_{\mathrm{O}}(g_0, L/a) = c(\theta, a/L)\, \frac{g_{\mathrm{O}}(L/2, \theta)}{\sqrt{g_1(\theta)}}\bigg|_{m=0}\,. \tag{3.11}$$

The factor $c(\theta, a/L)$ is chosen such that Z_{O} takes the correct value at tree-level, $Z_{\mathrm{O}}(0, L/a) = 1$. Therefore it is defined as

$$c(\theta, a/L) \equiv \frac{\sqrt{g_1(\theta)}}{g_{\mathrm{O}}(L/2, \theta)}\bigg|^{\mathrm{tree}}_{m_0=0}\,. \tag{3.12}$$

In this expression g_1 is the two-point function defined in eq. (2.5). The other two-point function, g_{O}, is either g_{12} or g_{44} (cf. eq. (3.10)), depending if we consider the SSF of the operator O^a_{12} or O^a_{44}. In order to determine the renormalization prescription completely, a value of θ has to be chosen. In particular, we consider here two cases, $\boldsymbol{\theta} = (0.5, 0.5, 0.5)$

and $\boldsymbol{\theta} = (1, 0, 0)$. The reason for studying the case with $\boldsymbol{\theta} = (1, 0, 0)$ is that this is the only choice with $\boldsymbol{\theta} \neq \mathbf{0}$ for which there are data available from the standard SF [7] which thus allows us to test the continuum limit of the χSF. Although there are no SF data available for the choice $\boldsymbol{\theta} = (0.5, 0.5, 0.5)$, we have also analyzed this setup, since this is the usual choice when computing quantities within the SF formulation, as it was shown with the results presented in sec. 2. Moreover, this additional choice for the parameter $\boldsymbol{\theta}$ allows us to check the differences in the relative statistical errors when changing renormalization prescription through $\boldsymbol{\theta}$. All correlation functions are evaluated at $x_0 = T/2$, where $T = L$ is the time extent of the lattice. The scale factor is always set to $s = 2$.

Given a fixed value of the renormalization scale, defined through $\overline{g}^2(L) = u$, and a fixed value of the lattice spacing a, leading to a fixed value of L/a, the lattice SSF of O, defined in the chiral limit, is given as

$$\Sigma_{\mathrm{Z_O}}(s, u, a/L) = \frac{Z_{\mathrm{O}}(g_0, sL/a)}{Z_{\mathrm{O}}(g_0, L/a)}\Big|_{m=0,\, \overline{g}^2(L)=u} . \tag{3.13}$$

In the continuum limit the SSF is finite and takes the value

$$\sigma_{\mathrm{Z_O}}(s, u) = \lim_{a\to 0} \Sigma_{\mathrm{Z_O}}(s, u, a/L) = \frac{O_{\mathrm{R}}(L)}{O_{\mathrm{R}}(sL)}\Big|_{\overline{g}^2(L)=u} , \tag{3.14}$$

with $O_{\mathrm{R}}(L)$ the renormalized operator at a given value of the physical scale $1/L$ computed in the χSF renormalization scheme.

We employ the definitions given above and the chosen renormalization prescription, to determine the renormalization factors of the operators O^a_{12} and O^a_{44} within the χSF scheme at finite lattice spacing. Results are presented for several β-values and at three values of the renormalization scale, $1/L$. In particular, at the values such that $\overline{g}^2 = 0.9944$, $\overline{g}^2 = 2.4484$ and $L = 1.436\, r_0$. These results are presented in tab. A.6 and tab. A.7 for O^a_{12} and O^a_{44}, respectively. In both cases we show results at $\boldsymbol{\theta} = (0.5, 0.5, 0.5)$ and $\boldsymbol{\theta} = (1, 0, 0)$.

Concerning our results for the Z-factors in the χSF scheme, tab. A.6 and tab. A.7, at the three values of the renormalization scale and for all values of the lattice spacing that we have analyzed, we can make some interesting observations. For any of the two operators, O^a_{12} or O^a_{44}, the relative statistical errors in the renormalization constants, $\Delta Z_{\mathrm{O}}/Z_{\mathrm{O}}$, are always smaller for $\boldsymbol{\theta} = (1, 0, 0)$ than for $\boldsymbol{\theta} = (0.5, 0.5, 0.5)$ by nearly a factor of 2. Moreover, at fixed values of all parameters, the relative errors in $Z_{\mathrm{O}_{44}}$ are always slightly larger than those of $Z_{\mathrm{O}_{12}}$. These results are consistent with the pattern discussed previously in [7] within the standard SF setup, where it was shown that the relative statistical errors in $Z_{\mathrm{O}_{12}}$ and $Z_{\mathrm{O}_{44}}$ increase when the value of $\boldsymbol{\theta}$ decreases in modulus, for values such that the modulus of $\boldsymbol{\theta}$ is smaller or equal than 1, as it is our case here. There it was also shown that the errors in $Z_{\mathrm{O}_{44}}$ are slightly larger than those in $Z_{\mathrm{O}_{12}}$, which is consistent with what we observe from our χSF data.

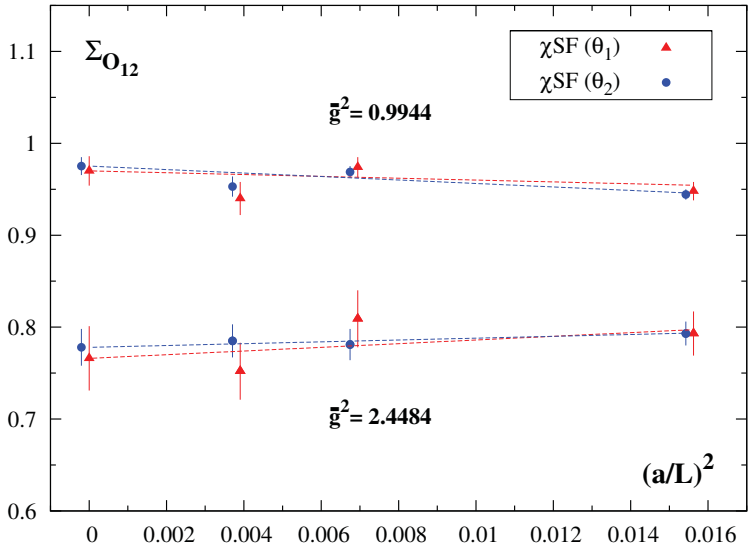

Fig. 4. Continuum limit extrapolation of the SSF of the operator O_{12}. Only χSF data are shown, both for $\theta_1 \equiv \boldsymbol{\theta} = (0.5, 0.5, 0.5)$ and $\theta_2 \equiv \boldsymbol{\theta} = (1, 0, 0)$, at the intermediate and perturbative scales. The extrapolations to the continuum limit, represented by dashed lines, are linear in $(a/L)^2$, see also tab. A.10 and tab. A.11. The values in the continuum limit are also plotted. The data for θ_2 have been plotted slightly displaced to the left.

At the two most perturbative couplings, $\overline{g}^2 = 0.9944$ and $\overline{g}^2 = 2.4484$, we have determined the lattice SSFs for both operators, whose values are shown in tab. A.8 for $\boldsymbol{\theta} = (0.5, 0.5, 0.5)$ and in tab. A.9 for $\boldsymbol{\theta} = (1, 0, 0)$. In tab. A.9 we have also added the values obtained for the lattice SSFs using the SF scheme with standard and non-perturbatively improved Wilson fermions. These values were taken from [7], where data are available only at the intermediate coupling, $\overline{g}^2 = 2.4484$.

To perform the continuum limit we have performed fits of the lattice data in tab. A.8 and tab. A.9, linear in $(a/L)^2$ for the χSF formulation and linear in a/L for the SF with standard and improved Wilson fermions. We have performed linear fits in a/L for the SF data even in the formulation of improved Wilson fermions because, although the action is improved in this setup, the twist-2 operators themselves are not. This is actually a major advantage of the χSF as a non-perturbative renormalization scheme: it is not necessary for this setup to determine additional counterterms to the operators, since this formulation preserves bulk automatic O(a) improvement, up to boundary effects which are expected to be small. The results of the fits are presented in tab. A.10 and tab. A.11.

The data for the lattice SSFs, tab. A.8 and tab. A.9, are plotted in fig. 4, fig. 5, fig. 6 and fig. 7, where we show the continuum limit approach of all SSFs that we have computed. In these figures we have also plotted the corresponding values of the SSFs in the continuum

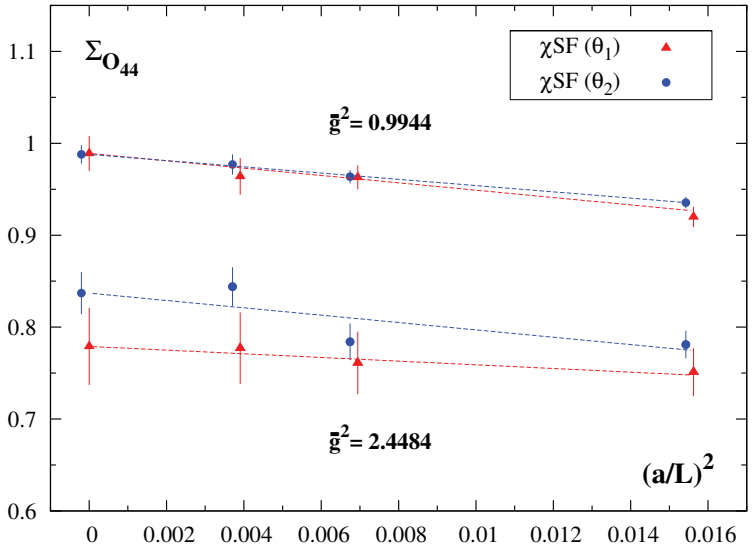

Fig. 5. Continuum limit extrapolation of the SSF of the operator O_{44}. Only χSF data are shown, both for $\theta_1 \equiv \boldsymbol{\theta} = (0.5, 0.5, 0.5)$ and $\theta_2 \equiv \boldsymbol{\theta} = (1, 0, 0)$, at the intermediate and perturbative scales. The extrapolations to the continuum limit, represented by dashed lines, are linear in $(a/L)^2$, see also tab. A.10 and tab. A.11. The values in the continuum limit are also plotted. The data for θ_2 have been plotted slightly displaced to the left.

limit and the fitting curves for the χSF case, as given in tab. A.10 and tab. A.11.

In fig. 4 and fig. 5 we show the continuum limit approach of the SSFs of the operators O^a_{12} and O^a_{44}, respectively, within the χSF scheme. In both figures we plot the results for both values of $\boldsymbol{\theta}$ and the two scales where we have computed the SSFs. Results are presented as a function of $(a/L)^2$, since only χSF data are considered. We can conclude, from these figures and the corresponding tables, that the cutoff effects in the χSF SSFs are consistent with $O(a^2)$ and are, in fact small. We can also see that the discretization effects are similar for different values of the renormalized coupling and $\boldsymbol{\theta}$. Note that the values in the continuum limit for different values of $\boldsymbol{\theta}$ are not expected to agree, since different $\boldsymbol{\theta}$ values correspond to different renormalization prescriptions.

In fig. 6 and fig. 7 we compare the results for the SSFs of O^a_{12} and O^a_{44} as obtained from the three formulations, χSF and SF with standard and improved Wilson fermions. Only the data at the intermediate coupling and for $\boldsymbol{\theta} = (1, 0, 0)$ are plotted. For a comparison with the SF, the data are plotted here as a function of a/L, although the values in the continuum limit for the χSF have been obtained from linear fits in $(a/L)^2$. As stated above, although the lattice data for the SF have been taken from [7], in this work we have performed our own fits towards the continuum limit. Results, for the three formulations, may be infered from tab. A.11. Additionally in tab. A.10 we show the results at $\boldsymbol{\theta} = (0.5, 0.5, 0.5)$ only

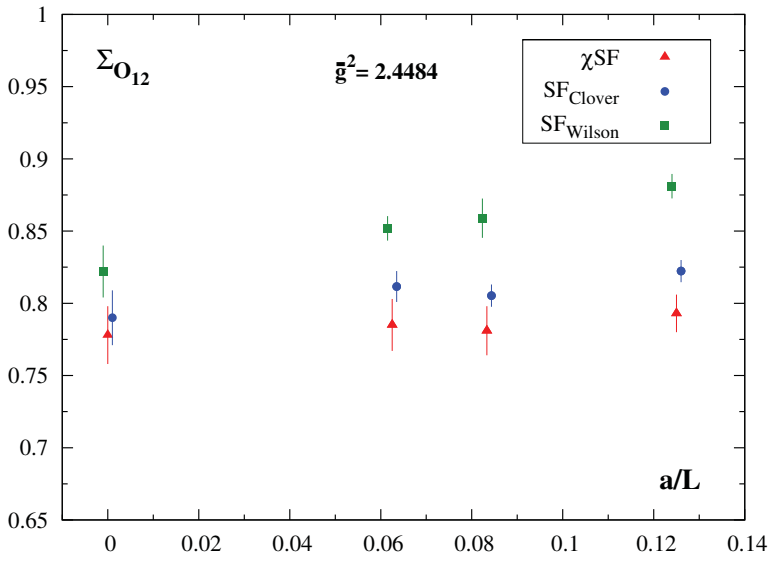

Fig. 6. Continuum limit approach of the SSF of the operator O_{12}. Data are shown for the χSF with standard Wilson fermions and for the SF with improved and standard Wilson fermions, at the intermediate scale and for $\boldsymbol{\theta} = (1, 0, 0)$. The continuum limit is performed according to tab. A.11: linear in $(a/L)^2$ for the χSF and linear in a/L for the SF with Wilson and clover improved Wilson regularizations. The continuum limit values are also plotted. The data from the SF have been plotted slightly displaced to the right and left, respectively, for the improved and unimproved formulations.

for the χSF formulation. There is a good agreement within statistical errors between the χSF and the improved SF formulations in the continuum limit.

In summary, we can conclude that there is agreement, within statistical errors, in the continuum limit amongst the results from the three formulations and therefore, the universality of the continuum limit is confirmed also through the SSFs of the twist-2 operators. Additionally, we observe that the scaling behavior of the SSFs obtained from the χSF is consistent with leading $O(a^2)$ discretization effects, which, furthermore, turn out to be rather small.

4 Renormalization factors at the matching scale

With Wilson twisted mass (Wtm) fermions the bare vector Ward identity [22] is exactly satisfied if one uses a point-split vector current. This implies that $Z_\mu = Z_P^{-1}$.

In the following we denote M the RGI quark mass, $\mu_q(g_0)$ the bare quark mass and $\overline{\mu}_q(L)$

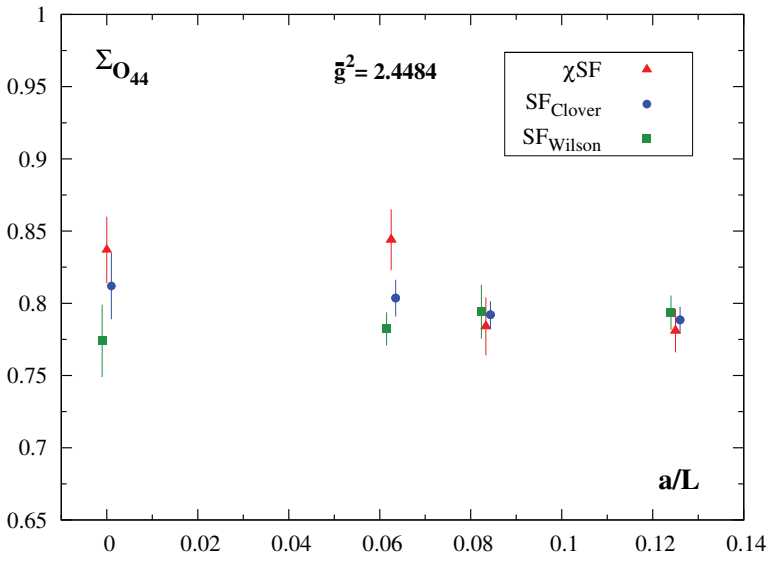

Fig. 7. Continuum limit approach of the SSF of the operator O_{44}. Data are shown for the χSF with standard Wilson fermions and for the SF with improved and standard Wilson fermions, at the intermediate scale and for $\boldsymbol{\theta} = (1, 0, 0)$. The continuum limit is performed according to tab. A.11: linear in $(a/L)^2$ for the χSF and linear in a/L for the SF with both regularizations. The continuum limit values are also plotted. The data from the SF have been plotted slightly displaced to the right and left, respectively, for the improved and unimproved formulations.

the renormalized running quark mass at the value $1/L$ of the renormalization scale.

The renormalized quark mass is given by

$$\overline{\mu}_q(L) = Z_{\rm P}^{-1}(g_0, L)\mu_q(g_0)\,, \tag{4.1}$$

with $Z_{\rm P}$ the renormalization factor of the pseudoscalar density. The RGI quark mass, M, can be directly related to the bare quark mass, $\mu_q(g_0)$,

$$M = Z_{\rm M}(g_0)\mu_q(g_0)\,, \tag{4.2}$$

through a renormalization factor, $Z_{\rm M}(g_0)$, defined as the product of two terms as follows

$$Z_{\rm M}(g_0) = \left(\frac{M}{\overline{\mu}_q(L)}\right)\left(\frac{1}{Z_{\rm P}(g_0, L)}\right). \tag{4.3}$$

The first term, $M/\overline{\mu}_q(L)$, is regularization independent but depends on the renormalization scheme as well as on the matching scale $1/L$ [3]. The second term, $Z_{\rm P}^{-1}(g_0, L)$, depends

[3] The matching scale is the energy scale chosen to match the renormalized quark mass $\overline{\mu}_q(L)$

on both the renormalization scheme and the regulator. The dependence is such that the RGI Z-factor $Z_{\rm M}(g_0)$ does not depend on the renormalization scheme but only on the regularization. All dependence on the matching scale has also disappeared.

In the discussion above, all equations correspond to the continuum theory. When the lattice is used as a regularization scheme, the correct relation would be

$$M = Z_{\rm M}(g_0)\mu_q(g_0) + O(a^n)\,, \tag{4.4}$$

with $n = 1$ in case of unimproved formulations and $n = 2$ if improvement is at work.

The regularization independent part of $Z_{\rm M}(g_0)$, $M/\overline{\mu}_q(L)$, has already been determined in [6]. The value is known in the *continuum theory* and at the matching scale $L = 1.436\,r_0$. Once the continuum limit is performed this factor is then universal, i.e. regulator independent, and therefore, we can use it for our calculations without the need of a new computation, since both the SF and the χSF are equivalent formulations in the continuum theory. The value obtained in [6] for this regularization independent term, in the continuum limit, is

$$M/\overline{\mu}_q(L) = 1.157\,(15) \quad \text{at} \quad L = 1.436\,r_0\,, \tag{4.5}$$

which has a relative error of 1.3%.

This means we are only left with the computation of two quantities. One is the regularization dependent part of the total renormalization factor, $Z_{\rm P}^{-1}(g_0, L)$, which is to be computed at the matching scale L of eq. (4.5) for several values of β and within the χSF scheme. The other quantity is the bare quark mass, $\mu_q(g_0)$, which also has to be determined for a range of bare couplings as explained in detail below in sec. 5.

The determination of $Z_{\rm P}(g_0, L/a)$ from the χSF, at a certain value of the renormalization scale and for several values of the lattice spacing, has already been explained in the previous section and the results are given in tab. A.1, at three values of $1/L$ and two values of $\boldsymbol{\theta}$. Amongst the cases presented in tab. A.1, we are here interested only in the data corresponding to the matching scale, $L = 1.436\,r_0$, and $\boldsymbol{\theta} = (0.5, 0.5, 0.5)$. For such a choice of the parameters, we have computed $Z_{\rm P}(g_0, L/a)$ at several values of the lattice spacing in the β range $6.0 \leq \beta \leq 6.5$, which we recall in tab. B.1.

With these data we can now study the dependence of $Z_{\rm P}$ on β and determine a curve that describes this dependence in the relevant range of β i.e. $6.0 \leq \beta \leq 6.5$. We use the

with the bare quark mass $\mu_q(g_0)$, i.e. the energy scale where one computes $Z_{\rm P}(g_0, L)$.

polynomial fit to describe our data

$$\begin{aligned} Z_{\rm P}(g_0, L/a)_{L=1.436\,r_0} &= \sum_{i=0}^{2} z_i^{\rm P} (\beta - 6.0)^i \,, \\ \beta &= 6/g_0^2, \qquad 6.0 \le \beta \le 6.5 \,, \end{aligned} \tag{4.6}$$

with the coefficients presented in the second column of tab. B.2.

From these data we may also determine the β-dependence for $Z_{\rm M}$, by computing $Z_{\rm P}^{-1}$ and then multiplying the result by the regularization independent term $M/\overline{\mu}_q(L) = 1.157$, as given in eq. (4.5). This value has an uncertainty of 1.3% which will be added in quadrature only at the end of all calculations, after the extrapolation to the continuum limit has been carried out. The results for $Z_{\rm M}$ at each of the β values where we have performed simulations are summarized in tab. B.3 together with the values of $Z_{\rm P}^{-1}$.

The curve describing the dependence of $Z_{\rm M}$ on β is the following

$$\begin{aligned} Z_{\rm M}(g_0) &= \sum_{i=0}^{2} z_i^{\rm M} (\beta - 6.0)^i \,, \\ \beta &= 6/g_0^2, \quad 6.0 \le \beta \le 6.5 \,, \end{aligned} \tag{4.7}$$

with the coefficients presented in the third column of tab. B.2.

From eq. (4.6) and eq. (4.7), it is now possible to compute $Z_{\rm P}$ and $Z_{\rm M}$ at any value of β within the range $6.0 \le \beta \le 6.5$, which is the range of β where large volume simulations have been performed, namely $\beta = 6.00, 6.10, 6.20, 6.45$. For these simulations a number of bare quark masses were employed which we can here utilize to determine the renormalized quark massfrom our knowledge of $Z_{\rm P}$ and $Z_{\rm M}$. The relevant values of $Z_{\rm P}$ and $Z_{\rm M}$ at the chosen values of β are summarized in tab. B.4.

As we did for the case of the pseudoscalar density we determine the RGI Z-factors of the operators O_{12}^a and O_{44}^a using the χSF formulation. These factors then relate the bare and the RGI matrix elements of the corresponding operator.

We first study the dependence of the Z-factors on β, at the matching scale $L = 1.436\,r_0$, and determine the curve describing such a dependence. Performing a fit of the data for the Z-factors (tab. A.6 and tab. A.7) of the form,

$$\begin{aligned} Z_{\rm O}(g_0, L/a)_{L=1.436\,r_0} &= \sum_{i=0}^{2} z_i^{\rm REN} (\beta - 6.0)^i \,, \\ \beta &= 6/g_0^2, \qquad 6.0 \le \beta \le 6.5 \,, \end{aligned} \tag{4.8}$$

we obtain the fitting coefficients $z_i^{\rm REN}$ presented in tab. B.5 for the χSF and the SF with standard and improved Wilson fermions. In eq. (4.8), 'REN' stays for the particular setup

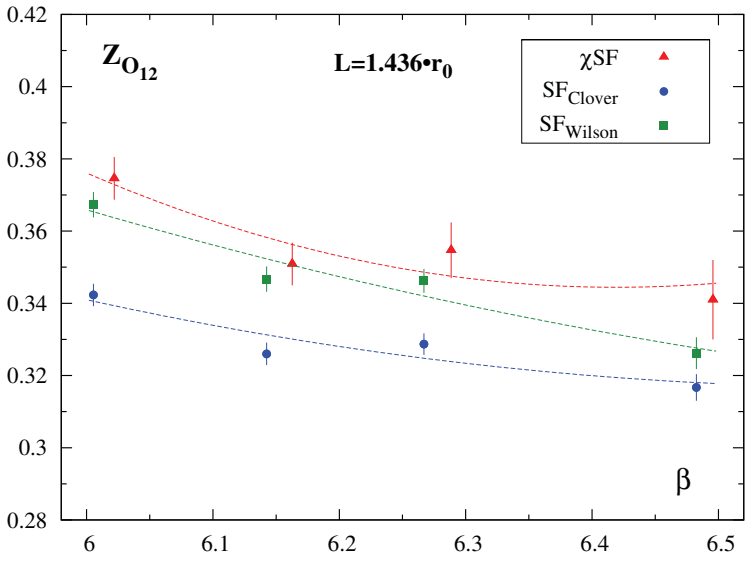

Fig. 8. Numerical results for $Z_{\mathrm{O}_{12}}(g_0, L/a)$ at scale $L = 1.436\, r_0$ and for several β values. $\boldsymbol{\theta} = (1,0,0)$. Results are shown for the χSF with standard Wilson fermions (cf. tab. A.6) and for the SF with standard and improved Wilson fermions, as taken from [23]. The fitting curves are also plotted (cf. eq. (4.8) and tab. (B.5)).

chosen: χSF, SF with standard Wilson fermions or SF with improved Wilson fermions. We have computed the Z-factors for O^a_{12} and O^a_{44} at $\boldsymbol{\theta} = (1,0,0)$ for all formulations and at $\boldsymbol{\theta} = (0.5, 0.5, 0.5)$ only for the χSF. These results are obtained from fits performed in this work for the three formulations, which for the SF are in agreement with the final results previously presented in [23]. We show the data together with the fitting curves, at $\boldsymbol{\theta} = (1,0,0)$ and for the three formulations, in fig. 8 and fig. 9 for $Z_{\mathrm{O}_{12}}$ and $Z_{\mathrm{O}_{44}}$, respectively.

As for the case of the pseudoscalar density it is possible to determine the RGI renormalization constants for the twist-2 operators from the knowledge of $Z^{\mathrm{REN}}(g_0, L/a)$ at a given value of the renormalization scale, $1/L$. For the twist-2 operators one defines, at the same value of the renormalization scale, $1/L$, the ultraviolet (UV) invariant SSF, $\sigma^{\mathrm{UV,REN}}_{\mathrm{INV,O}}(L)$, see ref. [24].

The UV invariant SSF of a certain operator is independent on the particular regularization but it depends on the renormalization scheme and the reference scale. In particular it is defined as,

$$\sigma^{\mathrm{UV,REN}}_{\mathrm{INV,O}}(L) = \frac{O^{\mathrm{RGI}}}{O_{\mathrm{R}}(L)}\,, \tag{4.9}$$

with $O_{\mathrm{R}}(L)$ the renormalized operator at scale $1/L$, defined in eq. (3.7) and the corre-

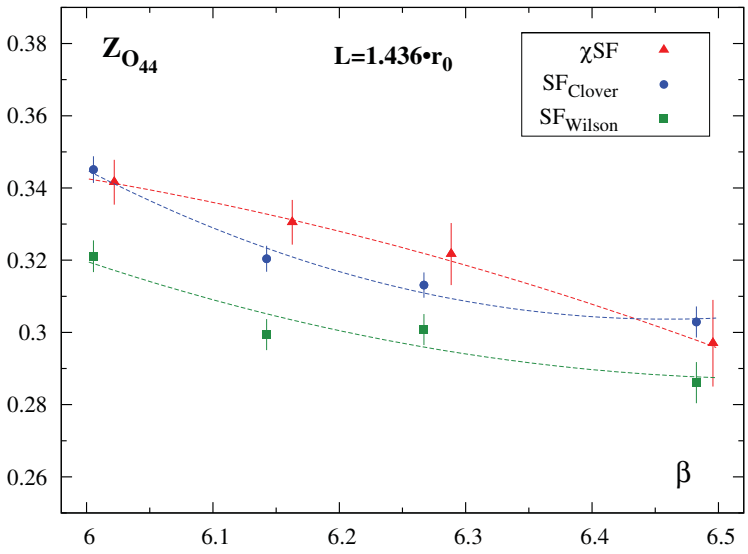

Fig. 9. Numerical results for $Z_{\mathrm{O}_{44}}(g_0, L/a)$ at scale $L = 1.436\, r_0$ and for several β values. $\boldsymbol{\theta} = (1,0,0)$. Results are shown for the χSF with standard Wilson fermions (cf. tab. A.7) and for the SF with standard and improved Wilson fermions, as taken from [23]. The fitting curves are also plotted (cf. eq. (4.8) and tab. (B.5)).

sponding RGI operator O^{RGI}. We note that the UV invariant SSF is the exact equivalent of the factor $\left(M/\overline{\mu}_q(L)\right)$ we have used for the RGI quark mass.

The RGI renormalization factor is scale and scheme independent but it depends on the particular regularization. It relates any bare matrix element of the bare operator, $O_{\mathrm{B}}(g_0)$, with the corresponding RGI matrix element and it is defined as follows,

$$Z_{\mathrm{O}}^{\mathrm{RGI}}(g_0) = \frac{Z^{\mathrm{REN}}(g_0, L/a)}{\sigma_{\mathrm{INV,O}}^{\mathrm{UV,REN}}(L)}\,. \tag{4.10}$$

In [7], the value of the UV invariant SSF was given for the operators O^a_{12} and O^a_{44} at scale $L = 1.436\, r_0$ and for $\boldsymbol{\theta} = (1,0,0)$. The values quoted there are

$$\sigma_{\mathrm{INV,O}_{12}}^{\mathrm{UV,SF}} = 0.242\,(8)\,, \qquad \sigma_{\mathrm{INV,O}_{44}}^{\mathrm{UV,SF}} = 0.221\,(9)\,. \tag{4.11}$$

Substituting in eq. (4.10) the values given in eq. (4.11) and the Z-factors in tab. A.6-A.7, at the matching scale $L = 1.436\, r_0$, the RGI Z-factors of the operators O^a_{12} and O^a_{44} are obtained and presented in tab. B.6. Results are shown only for $\boldsymbol{\theta} = (1,0,0)$. Since the UV invariant SSFs are only known at $\boldsymbol{\theta} = (1,0,0)$, the case of $\boldsymbol{\theta} = (0.5, 0.5, 0.5)$ is not discussed any longer in the present section. In the determination of the RGI Z-factors,

the error in the UV invariant SSF is not taken into account. This is a quantity in the continuum, and therefore its error is only considered at the end of all calculations, after the continuum limit has been performed. Its error is to be added in quadrature to the final value in the continuum limit.

A curve of $Z_{\rm O}^{\rm RGI}(g_0)$ as a function of β may be determined from the previous values in tab. B.6. The curve obtained is the following

$$\begin{aligned} &Z_{\rm O}^{\rm RGI}(g_0) = \sum_{i=0}^{2} z_i^{\rm RGI}(\beta - 6.0)^i\,, \\ &\beta = 6/g_0^2, \qquad 6.0 \leq \beta \leq 6.5\,, \end{aligned} \tag{4.12}$$

with the coefficients given in tab. B.7.

From the curves in eq. (4.8) and eq. (4.12) it is possible to determine, respectively, the Z-factors and the RGI Z-factors at any β-value within the range $6.0 \leq \beta \leq 6.5$. In particular, we show results for the Z-factors and RGI Z-factors in tab. B.8, at the β-values for which bare matrix elements have been evaluated in large volume simulations [25], keeping in mind a future determination of the corresponding renormalized matrix elements. The results presented in tab. B.8 correspond to $Z_{\rm O_{12}}$, $Z_{\rm O_{12}}^{\rm RGI}$, $Z_{\rm O_{44}}$ and $Z_{\rm O_{44}}^{\rm RGI}$, at $\boldsymbol{\theta} = (1, 0, 0)$. We also show in tab. B.8 the corresponding results for the SF formulation with improved and standard Wilson fermions. Note that, these data for $Z_{\rm O}(g_0, L/a)$ and $Z_{\rm O}^{\rm RGI}(g_0)$ are not supposed to be compared amongst the three formulations. The Z-factors and the RGI Z-factors depend on the regularization and therefore, only a comparison of the corresponding renormalized matrix elements in the continuum limit or the RGI matrix elements, depending on the case, would make sense. We nevertheless wanted to present here a calculation of the renormalization constants and the RGI Z-factors to demonstrate that the χSF can be used in practice to perform a non-perturbative renormalization of such non-trivial operators as considered in this work.

5 Strange quark mass

In this section we compute the RGI strange quark mass, $M_{\rm s}$, and the running strange quark mass in the $\overline{\rm MS}$-scheme at 2 GeV in quenched QCD. We use the χSF renormalization scheme with the setup discussed in the previous chapters together with the bare quark masses from large volume simulations with twisted mass fermions at maximal twist.

The purpose of this computation is to perform another check of the χSF formulation. In practice, we compute the quantity $r_0\,(M_{\rm s} + \hat{M})$, where $\hat{M} = (M_{\rm u} + M_{\rm d})/2$, r_0 is the Sommer parameter [26], and perform the continuum limit. The resulting continuum limit value, obtained from the χSF, is compared to the previously obtained value in [27], using the standard SF with improved Wilson fermions. We find that the continuum limit value

β	r_0/a	$a\mu_{\rm ref}$	$\mu_{\rm ref}\, r_0$
$\kappa_{\rm cr}^{\rm pion}$ definition			
6.00	5.368 (22)	0.01450 (59)	0.0778 (32)
6.10	6.324 (28)	0.01216 (40)	0.0769 (26)
6.20	7.360 (35)	0.01030 (34)	0.0758 (25)
6.45	10.458 (58)		
$\kappa_{\rm cr}^{\rm PCAC}$ definition			
6.00	5.368 (22)	0.01443 (51)	0.0775 (28)
6.20	7.360 (35)	0.01029 (27)	0.0757 (20)

Table 1
$\mu_{\rm ref}\, r_0$ at the value of the Kaon mass and for particular values of β. Results are shown for the pion and the PCAC definitions of the critical mass, see ref. [28]

obtained here agrees with the one in [27], which is an evidence of the universality of the continuum limit at the matching scale. Moreover, $r_0\,(M_{\rm s}+\hat{M})$ is expected to scale towards the continuum limit with leading $O(a^2)$ discretization errors, up to possible boundary effects. In fact, we will show that the scaling behavior is consistent with leading $O(a^2)$ discretization effects. This represents another test of bulk automatic $O(a)$-improvement and moreover it again gives an indirect indication that the boundary effects coming from d_s (see ref. [1]) are negligible, even at the large values of g_0 considered in this chapter.

To determine the strange quark mass we follow the strategy of ref. [27] and determine a reference bare quark mass $\mu_{\rm ref}$ defined by $2\mu_{\rm ref} = \mu_{\rm s} + \hat{\mu}$, where, $\hat{\mu} = (\mu_{\rm u} + \mu_{\rm d})/2$. The reference quark mass is then chosen such that the physical value of the kaon meson mass is reproduced.

To determine the values of the bare reference quark mass, $a\mu_{\rm ref}(g_0)$, at the values of β which are available from the large volume simulations and which overlap with the range of β described by our data, $6.0 \leq \beta \leq 6.5$, we use the data from from [28], where the pseudo-scalar mass, $m_{\rm PS}$, in lattice units was obtained using twisted mass Wilson fermions at maximal twist. (see tab. 1 and tab. 3 in ref. [28]). The pseudo-scalar mass range covered by these data set is $270{\rm MeV} < m_{\rm PS} < 1180{\rm MeV}$. Within this range, we may interpolate in the bare quark mass $a\mu_q$ at the experimental value Kaon mass, $m_{\rm K}$.

At each β value we perform a quadratic interpolation in the bare quark mass. We have cross checked that a linear interpolation with 3 data points closest to the interpolation point gives consistent results. The lattice spacing in physical units is obtained using the β dependence of r_0/a from ref. [29]. The final results for $\mu_{\rm ref}\, r_0$, together with the corresponding values of r_0/a and $a\mu_{\rm ref}$, are summarized in tab. 1.

Using the results for $Z_{\rm M}(g_0)$ obtained in sec. 4 and the reference quark mass computed

β	$Z_{\rm M}$	$r_0\,(M_{\rm s}+\hat{M})$
$\kappa_{\rm cr}^{\rm pion}$ definition		
6.00	2.1444 (55)	0.334 (14)
6.10	2.1733 (33)	0.334 (11)
6.20	2.1957 (42)	0.333 (11)
6.45	2.2236 (70)	
$\kappa_{\rm cr}^{\rm PCAC}$ definition		
6.00	2.1444 (55)	0.332 (12)
6.20	2.1957 (42)	0.3324 (88)

Table 2
$r_0\,(M_{\rm s}+\hat{M}) = Z_{\rm M}(2\mu_{\rm ref}\,r_0)$ at several values of β. Results are shown for the pion and the PCAC definitions of the critical mass.

above we can determine the RGI strange quark mass. The data at finite lattice spacing for the RGI reference quark mass are summarized in tab. 2.

In fig. 10 we plot our data for $r_0\,(M_{\rm s}+\hat{M})$ vs. $(a/r_0)^2$. We plot data obtained from two sets of large volume results corresponding to the two methods employed in ref. [28] to determine $\kappa_{\rm cr}$. The subtleties related to these 2 different choices are discussed in ref. [30] and refs. therein. For this work these two definitions simply correspond to two slighlty different discretization of the twisted mass action inducing slightly different O(a^2) cutoff effects in the physical quantities.

In the plot of fig. 10 we also show the fitting curves and the continuum limit values. These fits correspond to linear extrapolations in $(a/r_0)^2$. The data obtained from the SF with improved Wilson fermions [27] are also plotted for comparison.

The final values in the continuum limit, obtained from linear extrapolations in $(a/r_0)^2$, are presented in eq. (5.1) and eq. (5.2) for the PION and PCAC definitions of the critical mass, see ref. [28], respectively

$$\text{PION}: \quad r_0\,(M_{\rm s}+\hat{M})^{\chi{\rm SF}} = 0.332\,(28)\,, \tag{5.1}$$

$$\text{PCAC}: \quad r_0\,(M_{\rm s}+\hat{M})^{\chi{\rm SF}} = 0.333\,(23)\,. \tag{5.2}$$

The errors are obtained after adding in quadrature the 1.3% uncertainty in the factor $M/\mu(L)$. Thes values are perfectly consisten with the one obtained in [27]

$$r_0\,(M_{\rm s}+\hat{M})^{\rm SF} = 0.362\,(12)\,. \tag{5.3}$$

As can be seen from the previous results and the data in fig. 10, the SF data have relative errors which are about two times smaller than the errors obtained in our calculation

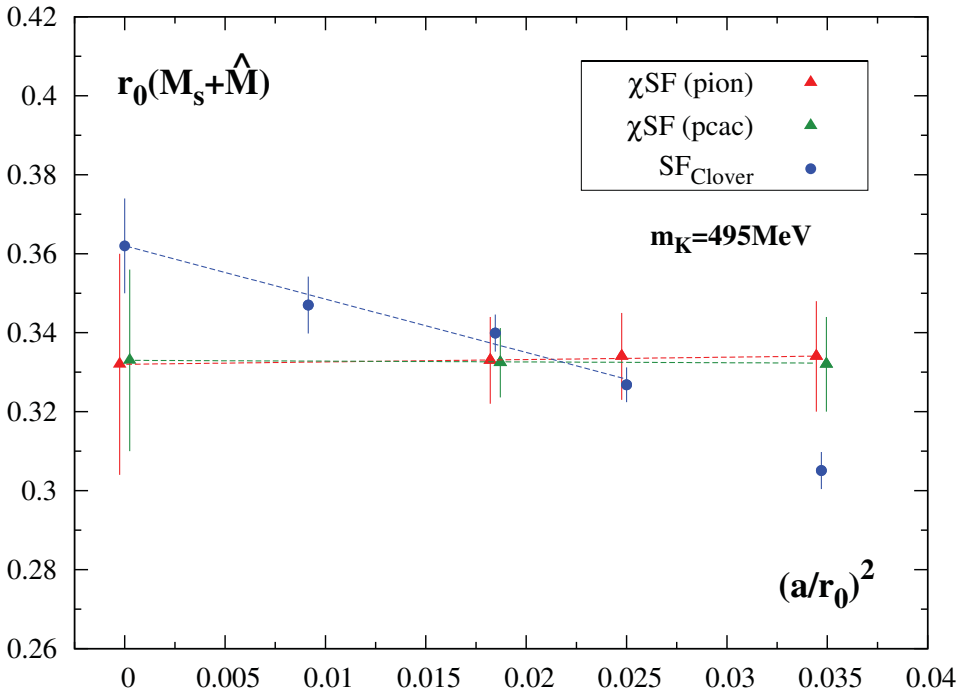

Fig. 10. $r_0(M_\mathrm{s}+\hat{M})$ vs. $(a/r_0)^2$, at the physical value of the Kaon mass, $m_\mathrm{K} = 495\mathrm{MeV}$. The extrapolations to the continuum limit are performed with linear fits in $(a/r_0)^2$. The values in the continuum limit are also plotted. Results are shown for the χSF with standard Wilson fermions, for the two definitions of the critical mass, and also for the SF with improved Wilson fermions [27]. The data for the χSF have been plotted slightly displaced to the right and left, respectively, for the PCAC and PION definitions of the critical mass.

using the χSF. The reason for this difference is the size of the statistical errors in the bare pseudo-scalar masses; if we compare the statistical errors in the bare pseudo-scalar masses from the large volume simulations using twisted mass fermions [28] with those of [27], we can see that the statistical errors in the last case are also about two times smaller than those of the former reference.

We can conclude that the values of the RGI reference quark mass, and therefore the RGI strange quark mass itself, determined using the SF and the χSF agree in the continuum limit. This is another test of the universality of the continuum limit, this time at the matching scale, $L = 1.436\, r_0$ and hence at a rather large value of the coupling. In particular, these results demonstrate that the χSF and twisted mass Wilson fermions at maximal twist are a valuable tool for the computation of renormalized quark masses.

Even if not necessary for the universality test, we compute for completeness the value of

the RGI strange quark mass, $M_{\rm s}$, in physical units and the running strange quark mass in the $\overline{\rm MS}$-scheme. As discussed in [27], chiral perturbation theory allows for a precise determination of ratios of masses of the three lightest quarks, u, d, s [31,32,33]. Such determinations led to

$$M_{\rm u}/M_{\rm d} = 0.553 \pm 0.043\,, \qquad M_{\rm s}/\hat{M} = 24.4 \pm 1.5\,, \tag{5.4}$$

with

$$\hat{M} \equiv \frac{1}{2}\,(M_{\rm u} + M_{\rm d})\,. \tag{5.5}$$

Considering these relations together with eq. (5.1) and eq. (5.2), we can determine the value of the RGI strange quark mass, $M_{\rm s}$. The final result in units of r_0 is

$$\text{PION}: \quad r_0\, M_{\rm s}^{\chi{\rm SF}} = 0.319\,(27)\,, \tag{5.6}$$

$$\text{PCAC}: \quad r_0\, M_{\rm s}^{\chi{\rm SF}} = 0.320\,(22)\,, \tag{5.7}$$

for the PION and PCAC definitions of $\kappa_{\rm cr}$, respectively. Repeating this analysis with the data in [27] we obtain,

$$r_0\, M_{\rm s}^{\rm SF} = 0.348\,(12)\,. \tag{5.8}$$

The value of the RGI strange quark mass can be now given in physical units,

$$\text{PION}: \quad M_{\rm s}^{\chi{\rm SF}} = 126\,(11)\,\text{MeV}\,, \tag{5.9}$$

$$\text{PCAC}: \quad M_{\rm s}^{\chi{\rm SF}} = 126\,(9)\,\text{MeV}\,, \tag{5.10}$$

and for the SF,

$$M_{\rm s}^{\rm SF} = 137\,(5)\,\text{MeV}\,. \tag{5.11}$$

Using the conversion factor between the RGI mass and the running mass in the $\overline{\rm MS}$-scheme, the running strange quark mass in the $\overline{\rm MS}$-scheme can be directly determined. At a value of the energy scale of 2 GeV and up to 4-loop, the flavor independent conversion factor is

$$\overline{m}^{\overline{\rm MS}}(2\,\text{GeV})/M = 0.72076\,. \tag{5.12}$$

As a result, the strange quark mass at 2 GeV with a 4-loop running in the $\overline{\rm MS}$-scheme is the following, as determined from the χSF and the SF,

$$\chi\text{SF}: \quad \overline{\mu}_{\rm s}^{\overline{\rm MS}}(2\,\text{GeV}) = 91\,(6)\,\text{MeV}\,, \tag{5.13}$$

$$\text{SF}: \quad \overline{m}_{\rm s}^{\overline{\rm MS}}(2\,\text{GeV}) = 99\,(4)\,\text{MeV}\,, \tag{5.14}$$

where we quote as our best result the strange quark mass obtained from the PCAC definition of $\kappa_{\rm cr}$.

6 Conclusions

In this work we have made a detailed study of several applications of the χSF scheme proposed in ref. [15] with quenched Wilson fermions. Using our results [1] for the non-perturbative tuning of the χSF we have performed a number of scaling studies of the χSF. More specifically we have analyzed step-scaling functions of the pseudoscalar densities and of twist-2 operators at a perturbative and an intermediate value of the renormalized coupling. All our results show perfect agreement in the continuum limit with the results using standard SF scheme, if the same renormalization conditions are adopted. Additionally all our data are consistent with scaling violations of only $O(a^2)$ thus demonstrating the bulk $O(a)$ improvement of the χSF scheme.

We remark that for the twist-2 operators this is an important result because to improve in the standard SF scheme the twist-2 operators studied in this work would have required a non-perturbative computation of additional improvement coefficients proportional to dimension 5 operators. The automatic $O(a)$ improvement found here with the example of the twist-2 operators is an important result which can be taken over to other observables. It demonstrates that automatic $O(a)$ improvement is at work and that with the χSF scheme in combination with maximally twisted mass fermions the somewhat tedious computation of operator specific improvement coefficients can be avoided.

Finally we have performed the continuum limit of the renormalized strange quark mass within the χSF scheme. In this case as well the result in the continuum limit is consistent with previous results obtained with non-perturbatively improved Wilson fermions and the standard SF scheme, thus confirming the χSF scheme as a non-perturbative method to perform renormalization on the lattice.

We conclude that the finite volume χSF scheme is a valuable alternative to infinite volume renormalization schemes such as the RI-MOM [34,35] or the X-space schemes [36,37]. It is on the same footing as the standard SF scheme [2,3,4] which has been applied successfully as a non-perturbative renormalization scheme. We believe therefore that the χSF scheme is a practical and theoretically well defined framework that can be used as a non-perturbative renormalization scheme for large volume calculations of bare operators.

Acknowledgments
We thank S. Sint and B. Leder for many useful discussions. We also acknowledge the support of the computer center in DESY-Zeuthen and the NW-grid in Lancaster. This work has been supported in part by the DFG Sonderforschungsbereich/Transregio SFB/TR9-03. This manuscript has been coauthored by Jefferson Science Associates, LLC under Contract No. DE-AC05-06OR23177 with the U.S. Department of Energy.

A Tables of numerical results for the step-scaling functions

		$\boldsymbol{\theta} = (0.5, 0.5, 0.5)$		$\boldsymbol{\theta} = (1, 0, 0)$	
L/a	β	$Z_{\rm P}(g_0, L/a)$	$Z_{\rm P}(g_0, 2L/a)$	$Z_{\rm P}(g_0, L/a)$	$Z_{\rm P}(g_0, 2L/a)$
Hadronic scale: $L = 1.436\, r_0$					
8	6.0219	0.5385 (12)		0.5432 (12)	
10	6.1628	0.5264 (12)		0.5310 (12)	
12	6.2885	0.5272 (16)		0.5321 (17)	
16	6.4956	0.5187 (22)		0.5245 (21)	
Intermediate scale: $\overline{g}^2 = 2.4484$					
8	7.0197	0.68509 (95)	0.6199 (14)	0.68850 (93)	0.6241 (13)
12	7.3551	0.6735 (13)	0.6082 (19)	0.6788 (12)	0.6142 (21)
16	7.6101	0.6672 (16)	0.5991 (22)	0.6737 (16)	0.6015 (22)
Perturbative scale: $\overline{g}^2 = 0.9944$					
8	10.3000	0.82689 (56)	0.80129 (84)	0.83007 (58)	0.80358 (84)
12	10.6086	0.81651 (88)	0.78549 (84)	0.81924 (82)	0.79008 (80)
16	10.8910	0.8110 (10)	0.7820 (14)	0.8136 (11)	0.7802 (15)

Table A.1: Renormalization factors of the pseudo-scalar density, $Z_{\rm P}$, at $\boldsymbol{\theta} = (0.5, 0.5, 0.5)$ and $\boldsymbol{\theta} = (1, 0, 0)$. Results are shown for the χSF with standard Wilson fermions at three values of the renormalization scale and for several values of the lattice spacing.

$\Sigma_{\rm P}(2, u, a/L)$			
L/a	χSF	SF (Clover)	SF (Wilson)
Intermediate scale: $\overline{g}^2 = 2.4484$			
8	0.9048 (23)	0.8945 (23)	0.8993 (20)
12	0.9030 (33)	0.8908 (23)	0.8924 (30)
16	0.8980 (39)	0.8998 (25)	0.9036 (32)
Perturbative scale: $\overline{g}^2 = 0.9944$			
8	0.9690 (12)	0.9633 (14)	0.9641 (12)
12	0.9620 (15)	0.9599 (19)	0.9632 (17)
16	0.9643 (22)	0.9622 (20)	0.9652 (22)

Table A.2: SSF of the pseudo-scalar density at finite lattice spacing, $\Sigma_{\rm P}(2, u, a/L)$. Results are shown for the χSF with standard Wilson fermions and also for the SF with improved and standard Wilson fermions [20] at two values of the renormalization scale and for several values of the lattice spacing. $\boldsymbol{\theta} = (0.5, 0.5, 0.5)$.

$\Sigma_{\rm P}(2, u, a/L)$	
L/a	χSF
Intermediate scale: $\overline{g}^2 = 2.4484$	
8	0.9065 (23)
12	0.9048 (35)
16	0.8929 (39)
Perturbative scale: $\overline{g}^2 = 0.9944$	
8	0.9681 (12)
12	0.9644 (14)
16	0.9590 (23)

Table A.3: SSF of the pseudo-scalar density at finite lattice spacing, $\Sigma_{\rm P}(2, u, a/L)$. Results are shown for the χSF with standard Wilson fermions at two values of the renormalization scale and for several values of the lattice spacing. $\boldsymbol{\theta} = (1, 0, 0)$.

	χSF	SF (Clover)	SF (Wilson)
Intermediate scale: $\overline{g}^2 = 2.4484$			
$\sigma_{\rm P}(2,u)$	0.8981 (41)	0.8968 (28)	0.8993 (58)
slope	0.44 (34)	-0.22 (27)	-0.007 (56)
χ^2/dof	0.5349	6.4083	6.8156
Perturbative scale: $\overline{g}^2 = 0.9944$			
$\sigma_{\rm P}(2,u)$	0.9595 (21)	0.9602 (22)	0.9644 (37)
slope	0.59 (18)	0.19 (19)	-0.004 (35)
χ^2/dof	2.4748	1.1258	0.5129

Table A.4: Continuum limit of the SSF of the pseudo-scalar density. Results are shown for the χSF with standard Wilson fermions and also for the SF with improved and standard Wilson fermions at two values of the renormalization scale. $\boldsymbol{\theta} = (0.5, 0.5, 0.5)$. These results correspond to linear fits of the data in tab. A.2. The fit is linear in a/L for the SF(Wilson) formulation while it is linear in $(a/L)^2$ for the χSF and SF(Clover) formulations.

	χSF
Intermediate scale: $\overline{g}^2 = 2.4484$	
$\sigma_{\rm P}(2,u)$	0.8942 (42)
slope	0.82 (34)
χ^2/dof	3.3471
Perturbative scale: $\overline{g}^2 = 0.9944$	
$\sigma_{\rm P}(2,u)$	0.9591 (21)
slope	0.59 (17)
χ^2/dof	1.8644

Table A.5: Continuum limit of the SSF of the pseudo-scalar density. Results are shown for the χSF with standard Wilson fermions at two values of the renormalization scale. $\boldsymbol{\theta} = (1, 0, 0)$. These results correspond to linear fits in $(a/L)^2$ of the data in tab. A.3.

		$\boldsymbol{\theta} = (0.5, 0.5, 0.5)$		$\boldsymbol{\theta} = (1, 0, 0)$	
L/a	β	$Z_{\rm O_{12}}(g_0, L/a)$	$Z_{\rm O_{12}}(g_0, 2L/a)$	$Z_{\rm O_{12}}(g_0, L/a)$	$Z_{\rm O_{12}}(g_0, 2L/a)$
Hadronic scale: $L = 1.436\, r_0$					
8	6.0219	0.395 (12)		0.3746 (59)	
10	6.1628	0.374 (13)		0.3509 (59)	
12	6.2885	0.348 (15)		0.3547 (77)	
16	6.4956	0.353 (21)		0.341 (11)	
Intermediate scale: $\overline{g}^2 = 2.4484$					
8	7.0197	0.6077 (80)	0.482 (13)	0.5675 (41)	0.4498 (64)
12	7.3551	0.613 (11)	0.495 (16)	0.5634 (58)	0.4401 (84)
16	7.6101	0.611 (14)	0.460 (16)	0.5587 (70)	0.4383 (84)
Perturbative scale: $\overline{g}^2 = 0.9944$					
8	10.3000	0.7989 (44)	0.7570 (68)	0.7717 (25)	0.7287 (36)
12	10.6086	0.7800 (66)	0.7597 (62)	0.7530 (35)	0.7295 (34)
16	10.8910	0.7762 (83)	0.730 (11)	0.7511 (45)	0.7161 (68)

Table A.6: Renormalization factors $Z_{\rm O_{12}}$ for $\boldsymbol{\theta} = (0.5, 0.5, 0.5)$ and $\boldsymbol{\theta} = (1, 0, 0)$. Results are shown for the χSF with standard Wilson fermions at three values of the renormalization scale and for several values of the lattice spacing.

		$\boldsymbol{\theta} = (0.5, 0.5, 0.5)$		$\boldsymbol{\theta} = (1, 0, 0)$	
L/a	β	$Z_{\mathrm{O}_{44}}(g_0, L/a)$	$Z_{\mathrm{O}_{44}}(g_0, 2L/a)$	$Z_{\mathrm{O}_{44}}(g_0, L/a)$	$Z_{\mathrm{O}_{44}}(g_0, 2L/a)$
Hadronic scale: $L = 1.436\, r_0$					
8	6.0219	0.319 (10)		0.3416 (62)	
10	6.1628	0.307 (10)		0.3305 (62)	
12	6.2885	0.280 (14)		0.3217 (86)	
16	6.4956	0.261 (19)		0.297 (12)	
Intermediate scale: $\bar{g}^2 = 2.4484$					
8	7.0197	0.5174 (75)	0.388 (12)	0.5382 (44)	0.4203 (71)
12	7.3551	0.532 (11)	0.404 (16)	0.5340 (64)	0.4189 (93)
16	7.6101	0.521 (14)	0.405 (17)	0.5236 (82)	0.4417 (86)
Perturbative scale: $\bar{g}^2 = 0.9944$					
8	10.3000	0.7369 (46)	0.6781 (71)	0.7529 (26)	0.7044 (39)
12	10.6086	0.7145 (64)	0.6882 (68)	0.7334 (37)	0.7068 (39)
16	10.8910	0.7114 (88)	0.686 (11)	0.7301 (51)	0.7135 (65)

Table A.7: Renormalization factors $Z_{\mathrm{O}_{44}}$ for $\boldsymbol{\theta} = (0.5, 0.5, 0.5)$ and $\boldsymbol{\theta} = (1, 0, 0)$. Results are shown for the χSF with standard Wilson fermions at three values of the renormalization scale and for several values of the lattice spacing.

χSF		
L/a	$\Sigma_{\mathrm{O}_{12}}(2, u, a/L)$	$\Sigma_{\mathrm{O}_{44}}(2, u, a/L)$
Intermediate scale: $\bar{g}^2 = 2.4484$		
8	0.793 (24)	0.751 (26)
12	0.809 (31)	0.761 (34)
16	0.752 (31)	0.777 (39)
Perturbative scale: $\bar{g}^2 = 0.9944$		
8	0.948 (10)	0.920 (11)
12	0.974 (11)	0.963 (13)
16	0.940 (18)	0.964 (20)

Table A.8: SSF of O_{12} and O_{44} at finite lattice spacing, $\Sigma_{\mathrm{O}_{12}}$ and $\Sigma_{\mathrm{O}_{44}}$. Results are shown for the χSF with standard Wilson fermions at two values of the renormalization scale and for several values of the lattice spacing. $\boldsymbol{\theta} = (0.5, 0.5, 0.5)$.

	$\Sigma_{O_{12}}(2,u,a/L)$			$\Sigma_{O_{44}}(2,u,a/L)$		
L/a	χSF	SF (Clover)	SF (Wilson)	χSF	SF (Clover)	SF (Wilson)
Intermediate scale: $\bar{g}^2 = 2.4484$						
8	0.793 (13)	0.8223 (77)	0.8811 (85)	0.781 (15)	0.7885 (91)	0.7935 (119)
12	0.781 (17)	0.8053 (77)	0.8589 (136)	0.784 (20)	0.7921 (94)	0.7942 (186)
16	0.785 (18)	0.8116 (107)	0.8519 (85)	0.844 (21)	0.8036 (127)	0.7823 (115)
Perturbative scale: $\bar{g}^2 = 0.9944$						
8	0.9443 (56)			0.9355 (62)		
12	0.9688 (64)			0.9637 (72)		
16	0.953 (11)			0.977 (11)		

Table A.9: SSF of O_{12} and O_{44} at finite lattice spacing, $\Sigma_{O_{12}}$ and $\Sigma_{O_{44}}$. Results are shown for the χSF with standard Wilson fermions and also for the SF [7] with improved and standard Wilson fermions at two values of the renormalization scale and for several values of the lattice spacing. $\boldsymbol{\theta} = (1,0,0)$.

χSF		
	O_{12}	O_{44}
Intermediate scale: $\bar{g}^2 = 2.4484$		
$\sigma_O(2,u)$	0.766 (35)	0.779 (42)
slope	2 (3)	-2 (4)
χ^2/dof	1.4081	0.0421
Perturbative scale: $\bar{g}^2 = 0.9944$		
$\sigma_O(2,u)$	0.970 (16)	0.989 (19)
slope	-1 (1)	-4 (2)
χ^2/dof	3.3364	0.2731

Table A.10: Continuum limit of the SSF, $\sigma_{O_{12}}$ and $\sigma_{O_{44}}$, of the operators O_{12} and O_{44}. Results are shown for the χSF with standard Wilson fermions at two values of the renormalization scale. $\boldsymbol{\theta} = (0.5, 0.5, 0.5)$. These results correspond to linear fits of the data in tab. A.8. The fits are linear in $(a/L)^2$.

	O_{12}			O_{44}		
	χSF	SF (Clover)	SF (Wil)	χSF	SF (Clover)	SF (Wil)
Intermediate scale: $\bar{g}^2 = 2.4484$						
$\sigma_{\rm O}(2,u)$	0.778 (20)	0.790 (19)	0.822 (18)	0.837 (23)	0.812 (23)	0.774 (25)
slope	1 (2)	0.25 (19)	0.47 (19)	-4 (2)	-0.19 (23)	0.17 (26)
χ^2/dof	0.0772	0.8338	0.0332	2.9018	0.2471	0.1586
Perturbative scale: $\bar{g}^2 = 0.9944$						
$\sigma_{\rm O}(2,u)$	0.9752 (97)			0.988 (10)		
slope	-1.89 (82)			-3.40 (88)		
χ^2/dof	2.9783			0.0534		

Table A.11: Continuum limit of the SSF, $\sigma_{\rm O_{12}}$ and $\sigma_{\rm O_{44}}$, of the operators O_{12} and O_{44}. Results are shown for the χSF with standard Wilson fermions and also for the SF with improved and standard Wilson fermions at two values of the renormalization scale. $\boldsymbol{\theta} = (1,0,0)$. These results correspond to linear fits of the data in tab. A.9. The fits are linear in $(a/L)^2$ for the χSF formulation while they are linear in a/L for the SF.

B Tables of numerical results for the renormalization factors

L/a	β	$Z_{\rm P}$
8	6.0219	0.5385 (12)
10	6.1628	0.5264 (12)
12	6.2885	0.5272 (16)
16	6.4956	0.5187 (22)

Table B.1: $Z_{\rm P}(g_0, L/a)$ at $L = 1.436\, r_0$ and for $\boldsymbol{\theta} = (0.5, 0.5, 0.5)$.

i	$z_i^{\rm P}$	$z_i^{\rm M}$
0	0.5394 (14)	2.1444 (55)
1	-0.077 (15)	0.321 (60)
2	0.078 (30)	-0.32 (12)

Table B.2: Coefficients of the beta dependence of $Z_{\rm P}(g_0, L/a)$ at the matching scale $L = 1.436\, r_0$ (cf. Eq. (4.6)) and $Z_{\rm M}(g_0)$ (cf. Eq. (4.7)). Results are shown for the χSF with standard Wilson fermions at $\boldsymbol{\theta} = (0.5, 0.5, 0.5)$.

L/a	β	$Z_{\rm P}^{-1}$	$Z_{\rm M}$
8	6.0219	1.8569 (41)	2.1484 (47)
10	6.1628	1.8995 (42)	2.1977 (49)
12	6.2885	1.8968 (59)	2.1946 (68)
16	6.4956	1.9279 (80)	2.2306 (93)

Table B.3: $Z_{\rm P}^{-1}(g_0, L/a)$ at $L = 1.436\, r_0$ and $Z_{\rm M}(g_0)$, for $\boldsymbol{\theta} = (0.5, 0.5, 0.5)$. Results are shown for the χSF formulation and for all the β values where simulations have been performed.

β	$Z_{\rm P}$	$Z_{\rm M}$
6.00	0.5394 (14)	2.1444 (55)
6.10	0.53240 (82)	2.1733 (33)
6.20	0.5270 (10)	2.1957 (42)
6.45	0.5203 (17)	2.2236 (70)

Table B.4: $Z_{\rm P}(g_0, L/a)$ at $L = 1.436\, r_0$ and $Z_{\rm M}(g_0)$, for $\boldsymbol{\theta} = (0.5, 0.5, 0.5)$. Results are presented for the χSF formulation at several β values, as determined from the curves in eq. (4.6) and eq. (4.7).

	$z_i(O_{12})$			$z_i(O_{44})$		
i	χSF	SF (Clover)	SF (Wilson)	χSF	SF (Clover)	SF (Wilson)
$\boldsymbol{\theta} = (0.5, 0.5, 0.5)$						
0	0.402 (14)			0.323 (12)		
1	-0.25 (15)			-0.12 (12)		
2	0.30 (29)			-0.02 (25)		
$\boldsymbol{\theta} = (1, 0, 0)$						
0	0.3761 (69)	0.3410 (31)	0.3659 (35)	0.3426 (73)	0.3450 (37)	0.3197 (44)
1	-0.151 (72)	-0.077 (31)	-0.102 (35)	-0.059 (77)	-0.180 (37)	-0.117 (44)
2	0.18 (15)	0.061 (62)	0.047 (70)	-0.07 (16)	0.196 (72)	0.105 (89)

Table B.5: Coefficients of the beta-dependence of $Z_{\rm O_{12}}$ and $Z_{\rm O_{44}}$ at the matching scale $L = 1.436\, r_0$. Results are shown for the χSF with standard Wilson fermions at $\boldsymbol{\theta} = (1, 0, 0)$ and $\boldsymbol{\theta} = (0.5, 0.5, 0.5)$ and also for the SF [23] with improved and standard Wilson fermions at $\boldsymbol{\theta} = (1, 0, 0)$.

		$Z^{\rm RGI}_{\rm O_{12}}(g_0)$			$Z^{\rm RGI}_{\rm O_{44}}(g_0)$		
L/a	β	χSF	SF (Clo)	SF (Wil)	χSF	SF (Clo)	SF (Wil)
8	6.0219	1.548 (24)	1.414 (13)	1.518 (14)	1.546 (28)	1.562 (17)	1.453 (20)
10	6.1628	1.450 (24)	1.347 (13)	1.433 (14)	1.495 (28)	1.450 (16)	1.355 (19)
12	6.2885	1.466 (32)	1.358 (12)	1.431 (14)	1.456 (39)	1.417 (16)	1.361 (19)
16	6.4956	1.409 (45)	1.309 (15)	1.348 (18)	1.344 (54)	1.371 (19)	1.295 (26)

Table B.6: RGI renormalization factors, $Z^{\rm RGI}_{\rm O_{12}}(g_0)$ and $Z^{\rm RGI}_{\rm O_{44}}(g_0)$ for $\boldsymbol{\theta} = (1,0,0)$. Results are shown for the χSF with standard Wilson fermions and the SF with improved and standard Wilson fermions, for several values of the lattice spacing. We have determined in this work the RGI Z-factors for the SF from the Z-factors given in [23].

	$z_i^{\rm RGI}(O_{12})$			$z_i^{\rm RGI}(O_{44})$		
i	χSF	SF (Clover)	SF (Wilson)	χSF	SF (Clover)	SF (Wilson)
0	1.554 (29)	1.409 (13)	1.512 (14)	1.550 (33)	1.561 (17)	1.447 (20)
1	-0.62 (30)	-0.32 (13)	-0.42 (14)	-0.27 (35)	-0.81 (17)	-0.53 (20)
2	0.74 (62)	0.25 (26)	0.19 (29)	-0.32 (72)	0.89 (33)	0.48 (40)

Table B.7: Coefficients of the beta-dependence of $Z^{\rm RGI}_{\rm O_{12}}(g_0)$ and $Z^{\rm RGI}_{\rm O_{44}}(g_0)$. Results are shown for the χSF with standard Wilson fermions and the SF with improved and standard Wilson fermions at $\boldsymbol{\theta} = (1,0,0)$.

β	$Z_{\rm O_{12}}$	$Z^{\rm RGI}_{\rm O_{12}}$	$Z_{\rm O_{44}}$	$Z^{\rm RGI}_{\rm O_{44}}$
	χSF			
6.00	0.3761 (69)	1.554 (29)	0.3426 (73)	1.550 (33)
6.10	0.3627 (40)	1.499 (17)	0.3361 (43)	1.521 (19)
6.20	0.3529 (49)	1.458 (20)	0.3283 (53)	1.486 (24)
6.45	0.3436 (82)	1.420 (34)	0.3031 (90)	1.371 (41)
	SF (Clover)			
6.00	0.3410 (31)	1.409 (13)	0.3450 (37)	1.561 (17)
6.10	0.3338 (20)	1.3793 (83)	0.3290 (23)	1.489 (10)
6.20	0.3279 (23)	1.3550 (95)	0.3168 (27)	1.433 (12)
6.45	0.3186 (30)	1.317 (12)	0.3035 (35)	1.373 (16)
	SF (Wilson)			
6.00	0.3659 (35)	1.512 (14)	0.3197 (44)	1.447 (20)
6.10	0.3562 (22)	1.4719 (91)	0.3091 (28)	1.399 (13)
6.20	0.3474 (25)	1.436 (10)	0.3005 (32)	1.360 (14)
6.45	0.3296 (36)	1.362 (15)	0.2884 (46)	1.305 (21)

Table B.8: $Z_{\rm O}(g_0, L/a)$ at scale $L = 1.436\, r_0$ and $Z^{\rm RGI}_{\rm O}(g_0)$, for O_{12} and O_{44}. $\boldsymbol{\theta} = (1,0,0)$. Results are presented for the χSF with standard Wilson fermions and the SF with improved and standard Wilson fermions.

References

[1] J.G. Lopez et al., (2012), 1208.4591.

[2] M. Luscher et al., Nucl. Phys. B384 (1992) 168, hep-lat/9207009.

[3] S. Sint, Nucl. Phys. B421 (1994) 135, hep-lat/9312079.

[4] M. Luscher, JHEP 05 (2006) 042, hep-lat/0603029.

[5] M. Luscher et al., Nucl. Phys. B413 (1994) 481, hep-lat/9309005.

[6] ALPHA, S. Capitani et al., Nucl. Phys. B544 (1999) 669, hep-lat/9810063.

[7] Zeuthen-Rome / ZeRo, M. Guagnelli et al., Nucl. Phys. B664 (2003) 276, hep-lat/0303012.

[8] C. Pena, S. Sint and A. Vladikas, JHEP 09 (2004) 069, hep-lat/0405028.

[9] ALPHA, M. Della Morte et al., Nucl. Phys. B713 (2005) 378, hep-lat/0411025.

[10] ALPHA, M. Della Morte et al., Nucl. Phys. B729 (2005) 117, hep-lat/0507035.

[11] PACS-CS Collaboration, S. Aoki et al., JHEP 0910 (2009) 053, 0906.3906.

[12] PACS-CS collaboration, S. Aoki et al., JHEP 1008 (2010) 101, 1006.1164.

[13] ALPHA, F. Tekin, R. Sommer and U. Wolff, Nucl. Phys. B840 (2010) 114, 1006.0672.

[14] R. Frezzotti and G.C. Rossi, JHEP 08 (2004) 007, hep-lat/0306014.

[15] S. Sint, Nucl. Phys. B847 (2011) 491, 1008.4857.

[16] J.G. Lopez, K. Jansen and A. Shindler, PoS LATTICE2008 (2008) 242, 0810.0620.

[17] J.G. Lopez et al., PoS LAT2009 (2009) 199, 0910.3760.

[18] S. Sint and B. Leder, PoS LATTICE2010 (2010) 265, 1012.2500.

[19] ETM, P. Boucaud et al., (2007), hep-lat/0701012.

[20] ALPHA, M. Guagnelli et al., JHEP 05 (2004) 001, hep-lat/0402022.

[21] A. Bucarelli et al., Nucl. Phys. B552 (1999) 379, hep-lat/9808005.

[22] ALPHA, R. Frezzotti et al., JHEP 08 (2001) 058, hep-lat/0101001.

[23] Zeuthen-Rome (ZeRo), M. Guagnelli et al., Eur. Phys. J. C40 (2005) 69, hep-lat/0405027.

[24] M. Guagnelli, K. Jansen and R. Petronzio, Phys.Lett. B459 (1999) 594, hep-lat/9903012.

[25] S. Capitani et al., Phys. Lett. B639 (2006) 520, hep-lat/0511013.

[26] R. Sommer, Nucl. Phys. B411 (1994) 839, hep-lat/9310022.

[27] ALPHA, J. Garden et al., Nucl. Phys. B571 (2000) 237, hep-lat/9906013.

[28] XLF, K. Jansen et al., JHEP 09 (2005) 071, hep-lat/0507010.

[29] ALPHA, M. Guagnelli, R. Sommer and H. Wittig, Nucl. Phys. B535 (1998) 389, hep-lat/9806005.

[30] A. Shindler, Phys. Rept. 461 (2008) 37, 0707.4093.

[31] J. Gasser and H. Leutwyler, Phys. Rept. 87 (1982) 77.

[32] H. Leutwyler, (1994), hep-ph/9406283.

[33] H. Leutwyler, Phys. Lett. B378 (1996) 313, hep-ph/9602366.

[34] G. Martinelli et al., Nucl. Phys. B445 (1995) 81, hep-lat/9411010.

[35] ETM, M. Constantinou et al., JHEP 08 (2010) 068, 1004.1115.

[36] V. Gimenez et al., Phys.Lett. B598 (2004) 227, hep-lat/0406019.

[37] K. Cichy, K. Jansen and P. Korcyl, (2012), 1207.0628.